LES/PDF for premixed combustion in the DNS limit

Ranjith R. Tirunagari & Stephen B. Pope

Taylor & Francis
Taylor & Francis Group

LES/PDF for premixed combustion in the DNS limit

Ranjith R. Tirunagari and Stephen B. Pope[*]

Sibley School of Mechanical and Aerospace Engineering, Cornell University, Ithaca, USA

We investigated the behaviour of the composition probability density function (PDF) model equations used in a large-eddy simulation (LES) of turbulent combustion in the direct numerical simulation (DNS) limit; that is, in the limit of the LES resolution length scale Δ (and the numerical mesh spacing h) being small compared to the smallest flow length scale, so that the resolution is sufficient to perform a DNS. The correct behaviour of a PDF model in the DNS limit is that the resolved composition fields satisfy the DNS equations, and there are no residual fluctuations (i.e. the PDF is everywhere a delta function). In the DNS limit, the treatment of molecular diffusion in the PDF equations is crucial, and both the 'random-walk' and 'mean-drift' models for molecular diffusion are investigated. Two test cases are considered, both of premixed laminar flames (of thickness δ_L). We examine the solutions of the model PDF equations for these test cases as functions of Δ/δ_L and h/δ_L. Each of the two PDF models has advantages and disadvantages. The mean-drift model behaves correctly in the DNS limit, but it is more difficult to implement and computationally more expensive. The random-walk model does not have the correct behaviour in the DNS limit in that it produces non-zero residual fluctuations. However, if the specified mixing rate Ω normalised by the reaction timescale τ_c is sufficiently large ($\Omega\tau_c \gtrsim 1$), then the residual fluctuations are less than 10% and the observed flame speed and thickness are close to their laminar values. Away from the DNS limit (i.e. $h/\delta_L \gtrsim 1$), the observed flame thickness scales with the mesh spacing h, and the flame speed scales with Ωh. For this case it is possible to construct a non-general specification of the mixing rate Ω such that the flame speed matches the laminar flame speed.

Keywords: PDF methods; large-eddy simulation; turbulent combustion; DNS limit; premixed flames

Nomenclature

Roman

C_D	mixing rate constant, Equation (36)
C_L	mixing rate constant, Equation (44)
C_m	mixing rate constant, Equation (10)
D	nozzle diameter
$\mathcal{D}$	molecular diffusivity
$\mathcal{D}_e$	effective diffusivity, Equation (7)
$\mathcal{D}_n$	numerical diffusivity, Equation (38)
$\mathcal{D}_r$	residual diffusivity

[*]Corresponding author. Email: s.b.pope@cornell.edu

$\widetilde{f}(\boldsymbol{\psi}; \mathbf{x}, t)$	density-weighted PDF of composition
h	mesh spacing
N	number of particles
$\mathbf{S}$	reaction source term
s_L	laminar flame speed
T	temperature
t	time
$\mathbf{U}$	fluid velocity
u_F	flame speed
v	specific volume
$\mathbf{W}(t)$	isotropic Wiener process
$\mathbf{X}^*(t)$	particle position
$\mathbf{x}$	position
Y_{OH}	mass fraction of OH
z	coordinate along the axis of the opposed nozzles

Greek

Δ	LES resolution length scale
δ	smallest flow length scale
δ_F	flame thickness, Equation (34)
δ_L	laminar flame thickness
ρ	fluid density
$\sigma_{\phi,\,\mathrm{max}}$	maximum residual standard deviation
τ_c	reaction timescale
$\boldsymbol{\phi}(\mathbf{x}, t)$	composition
$\boldsymbol{\psi}$	sample-space variables corresponding to $\boldsymbol{\phi}$
Ω	mixing rate, Equation (10)

Superscripts

$\boldsymbol{\phi}^*$	particle composition
$\widetilde{\boldsymbol{\phi}}$	resolved composition
$\widetilde{\boldsymbol{\phi}}^*$	resolved composition at particle position

Subscripts

T_b	burnt temperature
T_u	unburnt temperature

Abbreviations

LES	large-eddy simulation
PDF	probability density function
DNS	direct numerical simulation

1. Introduction

Probability density function (PDF) methods [1] are seeing increased use in conjunction with large-eddy simulation (LES) as an effective means of accounting for the turbulence–chemistry interactions occurring in turbulent combustion [2,3]. While most previous applications of LES/PDF have been to non-premixed combustion [4–6], recently there have been several applications to premixed turbulent combustion [7–10].

In LESs [11–13], modelled equations are solved for the larger-scale *resolved* motions, while the effects of the smaller-scale (unresolved) *residual* motions are modelled. A specified LES resolution length scale, Δ, demarcates the resolved and residual scales. The most common approach to LES is to define the resolved fields by a filtering operation, with Δ being the characteristic width of the filter [11,14]. However, as discussed below, for the present considerations, it is preferable to define the resolved fields in terms of conditional means [13,15].

In practice, the resolution length scale Δ is usually linked to the mesh spacing h used in the numerical solution of the LES equations, e.g. $\Delta = h$ or $\Delta = 2h$, which leads to a mingling of modelling and numerical errors [11,16]. However, it is important to retain the distinction between these two quantities, in particular so that numerically-accurate solutions can be considered for $h/\Delta \ll 1$.

An obviously-desirable property of an LES formulation is that it correctly converges to the direct numerical simulation (DNS) limit. That is, as the resolution scale Δ becomes small compared to the smallest flow length scale δ (so that the residual motions tend to zero), then the LES equations should yield the same solutions as those obtained from the fundamental conservation laws (e.g. the Navier–Stokes equations) that apply in a DNS. The purpose of this paper is to examine the behaviour of the composition PDF models in this DNS limit.

In a typical application of LES to a high-Reynolds-number flow, Δ/δ is large, and molecular transport has a negligible direct effect on the resolved fields: its primary effects are the dissipation of kinetic energy and the mixing of species below the resolved scale. For this reason, in LES, molecular transport is often neglected or treated in an unrealistically simplified way [17]. But in the DNS limit, molecular transport is a dominant process, and hence must be implemented correctly if the DNS limit is to be attained.

We now provide three reasons why it is important for LES/PDF models to converge correctly to the DNS limit.

First, in laboratory flames, the molecular diffusivity can be much larger than one might expect, given the typical flow Reynolds numbers of order 10,000. This is primarily because the molecular diffusivity $\mathcal{D}$ (of dimensions length squared divided by time) increases strongly with temperature T (e.g. as $T^{1.7}$), and hence at flame temperatures can be 30 times its value at room temperature. Kemenov and Pope [17] show that, in a typical LES of the Barlow and Frank flames [18], the molecular diffusivity is generally several times the residual diffusivity for temperatures above 1000 K.

Second, there is recent interest in premixed combustion in turbulent counter-flow burners [9,10,19]. When LES is applied to these flames, it is typically found that the resolution scale Δ is of the same order of magnitude as the laminar flame thickness, δ_L. Hence, the direct effects of molecular transport are important, as is the convergence to the DNS limit.

Third, as computer power continues to increase, it is becoming practicable to perform *high-fidelity* LES for a larger class of flows. Whereas, in conventional LES, the resolution scale Δ is chosen to resolve only the larger, energy-containing motions, in high-fidelity LES, Δ is chosen to be much smaller to provide partial resolution of the smallest-scale

processes [20]. For many occurrences of turbulent combustion, in which the rate-controlling processes are at the smallest scales, high-fidelity LES may be required in order to provide reliable simulations [3]. By definition, high-fidelity LES approaches the DNS limit, and hence for this purpose it is essential that the LES/PDF models used converge correctly in this limit.

The effects of molecular diffusion on the joint PDF of compositions can be decomposed into: *spatial transport*, which affects the mean compositions; and *mixing*, which decreases the composition variances, while not affecting the means. These two effects are modelled separately. Here it is sufficient to consider the simplest mixing model, namely the 'interaction by exchange with the mean' (IEM) model [21], which (like other models) causes the mixing to occur at a specified rate Ω. Molecular transport can be implemented in two ways, and we consider both, with details given in Section 2. These are referred to as the *Random-Walk* (RW) model and the *Mean-Drift* (MD) model.

In the DNS limit, the residual diffusivity $\mathcal{D}_r$ vanishes in comparison to the molecular diffusivity $\mathcal{D}$. However, the mixing rate Ω does not vanish, but remains as an important parameter.

We investigate the DNS limit by applying the LES/PDF model equations to two test cases, both of premixed laminar flames. The first is an idealised, unstrained, one-dimensional, freely-propagating, premixed laminar flame, with one-step chemistry. For this case, the LES/PDF equations are solved using a simple 1D MATLAB® code. The second case is a strained methane/air premixed laminar flame in an opposed jet configuration, in which a cold methane/air jet is opposed to a jet of hot combustion products. In this case the LES/PDF equations are solved using the same 3D code used in many previous applications of LES/PDF to turbulent flames, (including turbulent premixed flames in the present counter-flow configuration [10]) and the chemistry is described by a 16-species reduced mechanism.

The LES/PDF equations are solved by particle-mesh methods, using N particles, mesh spacing h, and time steps Δt. Except where mentioned explicitly otherwise, the number of particles can be considered to be sufficiently large, and the time step sufficiently small, so that the only significant numerical errors arise from the mesh spacing, h.

The focus of the investigation is on the solution of the LES/PDF equations as a function of Δ/δ_L, i.e. the ratio of the resolution length scale to the laminar flame thickness: the DNS limit corresponds to this ratio tending to zero. We consider both the numerically-accurate solutions (corresponding to small h/Δ), and also numerical solutions with h/Δ of order unity.

The remainder of the paper is organised as follows. In Section 2 we describe the two LES/PDF models considered, namely the random-walk model and the mean-drift model. In Section 3 we consider the correct behaviour in the DNS limit, and the behaviour of the LES/PDF equations corresponding to the MD and RW models. In Section 4 we describe the first of the two test problems considered, namely an idealised, unstrained, one-dimensional, freely-propagating laminar, premixed flame. Numerically-accurate solutions to the LES/PDF equations in the DNS limit are presented and discussed. These solutions are obtained using a mesh-free particle method that is described in Appendix A. Then, we present numerical solutions obtained using a conventional cloud-in-cell (CIC) particle/mesh method, which is described in Appendix B. In this case, the solutions depend on the specified normalised mesh size h/Δ. In Section 5 we describe the second test case of a strained methane/air opposed-jet, laminar, premixed flame. The numerically-accurate solution of the laminar-flow equations for this case is obtained using CHEMKIN-PRO [22]. The numerical solutions to the LES/PDF equations in the DNS limit are obtained using the

same 3D particle/mesh method used in many previous LES/PDF studies (e.g. [6,9]). Based on the results obtained and other considerations, in Section 6 we discuss the relative merits of the random-walk and mean-drift models. Conclusions are drawn in Section 7.

2. Composition PDF methods

2.1. *Governing equations*

We consider the standard case of a low-Mach-number, single-phase, turbulent reacting flow. As functions of position, $\mathbf{x}$, and time, t, the flow is described by the fields of velocity, $\mathbf{U}(\mathbf{x}, t)$, and composition, $\boldsymbol{\phi}(\mathbf{x}, t)$. In general, the n_ϕ components of the composition vector $\boldsymbol{\phi}$ can be taken to be the mass fractions of the n_s chemical species and the enthalpy. For the low-Mach-number flow considered, as far as the thermochemistry is concerned, the pressure can be approximated as being constant and uniform, and is not shown explicitly in the notation. Thus, the equations of state determining the density ρ and temperature T are of the form

$$\rho(\mathbf{x}, t) = \hat{\rho}(\boldsymbol{\phi}(\mathbf{x}, t)), \tag{1}$$

and

$$T(\mathbf{x}, t) = \hat{T}(\boldsymbol{\phi}(\mathbf{x}, t)). \tag{2}$$

The velocity field is governed by the usual equations for the conservation of mass and momentum. The focus here is on the composition field, which we take to be governed by the equation

$$\rho \frac{\mathrm{D}\boldsymbol{\phi}}{\mathrm{D}t} = \rho \frac{\partial \boldsymbol{\phi}}{\partial t} + \rho \mathbf{U} \cdot \nabla \boldsymbol{\phi} = \nabla \cdot (\rho \mathcal{D} \nabla \boldsymbol{\phi}) + \rho \mathbf{S}, \tag{3}$$

where $\mathbf{S}$ is the reaction source term (i.e. the rate of change of $\boldsymbol{\phi}$ due to chemical reactions), and $\mathcal{D}$ is the molecular diffusivity. Both $\mathbf{S}$ and $\mathcal{D}$ are known functions of $\boldsymbol{\phi}$. The form of the diffusion term embodies the assumption of unity Lewis numbers, which is discussed further below.

2.2. *LES/PDF formulation*

In an LES/PDF simulation of the flow considered, the primary quantities involved are the resolved density, $\langle \rho(\mathbf{x}, t) \rangle$, the density-weighted resolved velocity, $\widetilde{\mathbf{U}}(\mathbf{x}, t)$, and the density-weighted PDF, $\widetilde{f}(\boldsymbol{\psi}; \mathbf{x}, t)$, where $\boldsymbol{\psi}$ are the sample-space variables corresponding to $\boldsymbol{\phi}$.

While a decomposition of the composition field into resolved and residual components is not needed, it is nevertheless useful to consider the (density-weighted) resolved composition field defined as

$$\widetilde{\boldsymbol{\phi}}(\mathbf{x}, t) \equiv \int \widetilde{f}(\boldsymbol{\psi}; \mathbf{x}, t) \boldsymbol{\psi} \, \mathrm{d}\boldsymbol{\psi}, \tag{4}$$

where, here and below, the integration is over the whole of the composition space. The PDF then represents the residual fluctuations about this mean.

The most common way to define resolved fields is by filtering (see for example [11,14]) and then the PDF is, more correctly, the filtered density function (FDF) [23,24]. The less common alternative, and that considered here, is to define $\widetilde{f}(\boldsymbol{\psi}; \mathbf{x}, t)$ as the PDF of composition, conditional on the resolved velocity field [13,15]. For most purposes the difference between the two approaches is more conceptual than practical, with the same models being used regardless of the approach taken. However, when applying the LES-PDF equations in the DNS limit or to laminar flows, there is a major difference: with the conditioning approach there are no residual fluctuations $\boldsymbol{\phi}''$ about the resolved mean $\widetilde{\boldsymbol{\phi}}$; whereas, with the filtering approach, there are non-zero residual fluctuations, which scale with Δ. Clearly, in considering the DNS limit, it is far preferable to adopt the approach that has the simple limiting behaviour $\boldsymbol{\phi}'' = 0$ rather than that in which the limiting behaviour depends non-trivially on the non-physical parameter Δ.

For some purposes, it is more convenient to use the specific volume $v \equiv 1/\rho$ rather than the density. For example, the resolved density is obtained from the PDF by

$$\langle \rho(\mathbf{x}, t)\rangle^{-1} = \widetilde{v}(\mathbf{x}, t) = \int \widetilde{f}(\boldsymbol{\psi}; \mathbf{x}, t)\hat{v}(\boldsymbol{\psi})\, d\boldsymbol{\psi}, \tag{5}$$

where $\hat{v} \equiv 1/\hat{\rho}$ is the equation of state for specific volume.

2.3. *Exact PDF equation*

The exact evolution equation for the PDF $\widetilde{f}(\boldsymbol{\psi}; \mathbf{x}, t)$ is

$$\langle \rho \rangle \frac{\partial \widetilde{f}}{\partial t} + \langle \rho \rangle \widetilde{\mathbf{U}} \cdot \nabla \widetilde{f} = -\nabla \cdot (\langle \rho \rangle \widetilde{f} \langle \mathbf{U} - \widetilde{\mathbf{U}} \,|\, \boldsymbol{\psi} \rangle)$$
$$-\frac{\partial}{\partial \psi_\alpha}\left(\langle \rho \rangle \widetilde{f}\, [\langle v\nabla \cdot (\rho\mathcal{D}\nabla\phi_\alpha)\,|\,\boldsymbol{\psi}\rangle + S_\alpha(\boldsymbol{\psi})]\right) + R, \tag{6}$$

where $\langle \,\cdot\,|\, \boldsymbol{\psi} \rangle$ denotes the mean conditional on the composition and on the resolved velocity field. (This is the variable-density version of Equation (C10) of [13].) The term R is discussed in [13]: suffice it to say that it is generally taken to be zero, and it certainly is zero for the laminar test cases considered here.

2.4. *Lagrangian particle method*

In PDF methods, the modelling and numerical solution are usually performed using a Lagrangian particle method [1,2,11]. The position of the general particle is denoted by $\mathbf{X}^*(t)$, and its composition by $\boldsymbol{\phi}^*(t)$. The modelling is performed by specifying the evolution of these particle properties; and the PDF considered, $\widetilde{f}(\boldsymbol{\psi}; \mathbf{x}, t)$, is the density-weighted PDF of $\boldsymbol{\phi}^*(t)$ conditional on $\mathbf{X}^*(t) = \mathbf{x}$.

2.5. *Random-walk model*

In the random-walk (RW) model, the particle is specified to move with the resolved velocity, plus a random walk, the magnitude of which is determined by the *mean effective diffusivity* (which has dimensions of length squared divided by time). The molecular diffusivity is $\mathcal{D}$, and part of the LES modelling is to define a *residual diffusivity*, $\mathcal{D}_r$, which accounts for transport due to the residual motions. The effective diffusivity is then defined as their

sum:

$$\mathcal{D}_e \equiv \mathcal{D} + \mathcal{D}_r. \tag{7}$$

According to the RW model, the particle position evolves by the stochastic differential equation (SDE)

$$d\mathbf{X}^* = [\widetilde{\mathbf{U}} + \widetilde{v}\nabla(\langle\rho\rangle\widetilde{\mathcal{D}}_e)]^* \, dt + (2\widetilde{\mathcal{D}}_e^*)^{1/2} \, d\mathbf{W}, \tag{8}$$

where $\mathbf{W}(t)$ is an isotropic Wiener process. Note that $\mathcal{D}_e^*$ denotes the effective diffusivity based on the particle composition (and $\mathcal{D}_r$); whereas $\widetilde{\mathcal{D}}_e^*$ denotes the mean effective diffusivity evaluated at the particle location, i.e. it is a shorthand notation for $\widetilde{\mathcal{D}}_e(\mathbf{X}^*(t), t)$.

The evolution equation for the particle composition is

$$\frac{d\boldsymbol{\phi}^*}{dt} = -\Omega^*(\boldsymbol{\phi}^* - \widetilde{\boldsymbol{\phi}}^*) + \mathbf{S}(\boldsymbol{\phi}^*). \tag{9}$$

On the right-hand side, the first term is the IEM mixing model, and the second term is the reaction source term. The standard model for the mixing rate, Ω, is

$$\Omega = C_m \frac{\widetilde{\mathcal{D}}_e}{\Delta^2}, \tag{10}$$

where C_m is a model constant.

(Note that, in Equations 8 and 10, the diffusion coefficient and the mixing rate are based on the mean effective diffusivity, $\widetilde{\mathcal{D}}_e^*$. One can consider three additional model variants in which one or both of these quantities is instead based on the particle effective diffusivity, $\mathcal{D}_e^*$. Tests – for the case described in Section 4 – show that there are no qualitative differences between the four variants, and only modest quantitative differences.)

The PDF equation deduced from these particle equations is

$$\langle\rho\rangle\frac{\partial \widetilde{f}}{\partial t} + \langle\rho\rangle\widetilde{\mathbf{U}} \cdot \nabla\widetilde{f} = \nabla \cdot (\langle\rho\rangle\widetilde{\mathcal{D}}_e\nabla\widetilde{f}) - \frac{\partial}{\partial\psi_\alpha}\left(\langle\rho\rangle\widetilde{f}\left[-\Omega(\psi_\alpha - \widetilde{\phi}_\alpha) + S_\alpha(\boldsymbol{\psi})\right]\right), \tag{11}$$

where the summation convention applies to the repeated composition suffix α. Henceforth we refer to this as the RW-PDF equation.

Multiplying this PDF equation by $\boldsymbol{\psi}$ and integrating over the composition space, we obtain the implied conservation equation for the resolved composition:

$$\langle\rho\rangle\frac{\partial \widetilde{\boldsymbol{\phi}}}{\partial t} + \langle\rho\rangle\widetilde{\mathbf{U}} \cdot \nabla\widetilde{\boldsymbol{\phi}} = \nabla \cdot (\langle\rho\rangle\widetilde{\mathcal{D}}_e\nabla\widetilde{\boldsymbol{\phi}}) + \langle\rho\rangle\widetilde{\mathbf{S}}. \tag{12}$$

Note that the random walk (and in particular the drift term in Equation (8)) is constructed to yield the diffusion term in Equation (12); and, by construction, the IEM model does not (directly) affect the resolved composition $\boldsymbol{\phi}$, and hence the mixing rate Ω does not appear in Equation (12).

2.6. *Mean-drift model*

In the random-walk model, molecular transport is implemented via the random walk in the SDE for the particle position, $\mathbf{X}^*(t)$. In contrast, in the mean-drift (MD) model [25,26], molecular transport is implemented in the ODE for composition. The particle evolution equations for the MD model are

$$d\mathbf{X}^* = [\widetilde{\mathbf{U}} + \widetilde{v}\nabla(\langle\rho\rangle\widetilde{\mathcal{D}}_r)]^* \, dt + (2\widetilde{\mathcal{D}}_r^*)^{1/2} \, d\mathbf{W}, \tag{13}$$

$$\frac{d\boldsymbol{\phi}^*}{dt} = [\widetilde{v}\nabla \cdot (\langle\rho\rangle\widetilde{\mathcal{D}}\nabla\widetilde{\boldsymbol{\phi}})]^* - \Omega^*(\boldsymbol{\phi}^* - \widetilde{\boldsymbol{\phi}}^*) + \mathbf{S}(\boldsymbol{\phi}^*). \tag{14}$$

Thus, in the SDE for position (Equation 13) the random walk is based on $\widetilde{\mathcal{D}}_r$, and accounts solely for the transport due to the residual motions; and in the particle composition equation (Equation 14), the first term of the right-hand side accounts for transport by molecular diffusion.

For the mean-drift model, the corresponding PDF equation (deduced from Equations 13 and 14) is

$$\langle\rho\rangle\frac{\partial \widetilde{f}}{\partial t} + \langle\rho\rangle\widetilde{\mathbf{U}} \cdot \nabla\widetilde{f} = \nabla \cdot (\langle\rho\rangle\widetilde{\mathcal{D}}_r\nabla\widetilde{f}) - \frac{\partial}{\partial\psi_\alpha}\left(\langle\rho\rangle\widetilde{f}\left[\widetilde{v}\nabla \cdot (\langle\rho\rangle\widetilde{\mathcal{D}}\nabla\widetilde{\phi}_\alpha)\right.\right.$$
$$\left.\left. -\Omega(\psi_\alpha - \widetilde{\phi}_\alpha) + S_\alpha(\boldsymbol{\psi})\right]\right). \tag{15}$$

Henceforth we refer to this as the MD-PDF equation. The corresponding equation for the resolved composition is again Equation (12), i.e. it is identical to that for the random-walk model.

3. The PDF methods in the DNS limit

3.1. *The DNS limit*

The general idea of the DNS limit of an LES is simple and obvious: as the resolution length scale becomes small ($\Delta/\delta \ll 1$), it is highly desirable that the numerically-accurate solution to the LES model equations tends to the solution of the DNS equations. For the general case it is non-trivial to make this idea precise by quantifying the departure of the LES solution from the DNS solution as a function of Δ/δ.

The matter is more tractable for cases in which the flow is laminar (as in the test cases considered here), or in which Δ/δ is sufficiently small to resolve the velocity field fully. In these cases there is no randomness in the evolution of the composition field, and from the definitions of the resolved fields we therefore have simply

$$\widetilde{\mathbf{U}} = \mathbf{U}, \quad \langle\rho\rangle = \rho, \quad \widetilde{\boldsymbol{\phi}} = \boldsymbol{\phi}, \quad \widetilde{\mathcal{D}} = \mathcal{D}, \tag{16}$$

i.e. in the DNS limit the resolved quantities are equal to the instantaneous quantities. There are no composition fluctuations, so the PDF is the delta function:

$$\widetilde{f}(\boldsymbol{\psi}; \mathbf{x}, t) = \delta(\boldsymbol{\phi}(\mathbf{x}, t) - \boldsymbol{\psi}). \tag{17}$$

We observe that, in the DNS limit, the exact PDF equation (Equation 6) reduces to

$$\langle\rho\rangle\frac{\partial\widetilde{f}}{\partial t} + \langle\rho\rangle\widetilde{\mathbf{U}}\cdot\nabla\widetilde{f} = -\frac{\partial}{\partial\psi_\alpha}\left(\widetilde{f}\left[\nabla\cdot(\langle\rho\rangle\widetilde{\mathcal{D}}\nabla\widetilde{\phi}_\alpha) + \langle\rho\rangle S_\alpha(\boldsymbol{\psi})\right]\right). \quad (18)$$

Henceforth we refer to this as the DNS-PDF equation.

The question now to address is whether the LES-PDF equations (Equations 11 and 15) yield solutions consistent with the DNS limit.

Considering the resolved composition $\widetilde{\boldsymbol{\phi}}(\mathbf{x}, t)$ obtained from an LES, we define the difference between the LES and the DNS limit by

$$\epsilon_\phi(\Delta) = ||\widetilde{\boldsymbol{\phi}}(\mathbf{x}, t) - \boldsymbol{\phi}(\mathbf{x}, t)||, \quad (19)$$

where $||\cdot||$ denotes a suitable norm (e.g. the maximum absolute difference over all compositions, $\mathbf{x}$ and t). We say that the LES is *consistent* with the DNS provided that this difference tends to zero, i.e.

$$\lim_{\Delta/\delta\to 0}\epsilon_\phi(\Delta) = 0. \quad (20)$$

3.2. *The approach to the limit*

For an LES model, more than consistency is desirable: it is desirable also that the model have the *correct approach* to the DNS limit. Below, we encounter models for which the difference ϵ_ϕ varies quadratically as

$$\epsilon_\phi(\Delta) \sim \left(\frac{\Delta}{\delta}\right)^2. \quad (21)$$

This is an incorrect approach to the DNS limit, since (for the cases being considered) $\widetilde{\boldsymbol{\phi}}(\mathbf{x}, t)$ is independent of Δ/δ (provided that the velocity field is fully resolved).

The correct approach to the DNS limit is an important consideration in LES, since resolution is at a premium. Typically, the computational work W required to solve the LES equations varies as $W \sim (\Delta/\delta)^{-4}$. Consequently, if ϵ_ϕ varies quadratically with Δ/δ (Equation 21), then this error decreases slowly with increasing computational work as $W^{-1/2}$.

We say that a model *behaves correctly* in the DNS limit if it is consistent **and** it approaches the limit correctly.

3.3. *Numerical solutions and the DNS limit*

The preceding discussion pertains to the accurate solutions of the LES equations, whereas in practice the solutions are obtained numerically and hence contain a numerical error dependent upon the mesh spacing h. Consistency then requires that the numerical solutions of the LES equations converge to the DNS solutions as $\Delta/\delta \to 0$ and $h/\delta \to 0$. A remaining questions is: For consistency, is there a requirement on the ratio h/Δ as both h and Δ tend to zero? For the LES-PDF equations applied to laminar flames, this question is addressed in Section 4.6, with a possibly surprising answer.

3.4. *Residual covariance and the DNS limit*

The residual covariance is defined as

$$\widetilde{\phi''_\alpha \phi''_\beta} \equiv \int \widetilde{f}(\boldsymbol{\psi})(\psi_\alpha - \widetilde{\phi}_\alpha)(\psi_\alpha - \widetilde{\phi}_\beta)\, \mathrm{d}\boldsymbol{\psi}. \tag{22}$$

With the viewpoint taken here, that $\widetilde{f}$ is the PDF of the composition conditional on the resolved velocity field, in the DNS limit, this PDF is a delta function, Equation (17). Consequently, the residual covariance is zero.

   Note that if the alternative, filtering, viewpoint were taken, then, in the DNS limit, the residual covariance would instead be non-zero. With the usual definition of the filter width, to leading order in Δ, the residual covariance is

$$\widetilde{\phi''_\alpha \phi''_\beta} = \frac{\Delta^2}{12} \nabla \widetilde{\phi}_\alpha \cdot \nabla \widetilde{\phi}_\beta \tag{23}$$

(see Equation 13.157 of [11]). For the present purposes, it is clearly preferable to adopt the conditional PDF viewpoint so that the residual covariance is zero in the DNS limit.

3.5. *The mean-drift model in the DNS limit*

We now examine the behaviour of the mean-drift model in the DNS limit by comparing the MD-PDF equation (Equation 15) with the DNS-PDF equation (Equation 18).

   The first term on the right-hand side of the MD-PDF equation is absent from the DNS-PDF equation. This term represents turbulent transport by the residual motions, and is zero approaching the DNS limit (since $\mathbf{U} = \widetilde{\mathbf{U}}$, Equation 17). For the laminar cases considered below, it is certainly correct, therefore, to take the residual diffusivity $\widetilde{\mathcal{D}}_r$ to be zero. However, we note that, if instead the residual diffusivity were obtained from the standard Smagorinsky model and a specified turbulent Prandtl number, then this would lead to $\widetilde{\mathcal{D}}_r$ varying as $(\Delta/\delta)^2$, and hence would result in incorrect behaviour in the DNS limit.

   With $\widetilde{\mathcal{D}}_r$ taken to be zero, the MD-PDF equation can be written

$$\langle \rho \rangle \frac{\partial \widetilde{f}}{\partial t} + \langle \rho \rangle \widetilde{\mathbf{U}} \cdot \nabla \widetilde{f} = -\frac{\partial}{\partial \psi_\alpha} \left(\widetilde{f} \left[\nabla \cdot (\langle \rho \rangle \widetilde{\mathcal{D}} \nabla \widetilde{\phi}_\alpha) + \langle \rho \rangle S_\alpha(\boldsymbol{\psi}) - \langle \rho \rangle \Omega(\phi_\alpha - \widetilde{\phi}_\alpha) \right] \right). \tag{24}$$

This is identical to the DNS-PDF equation except for the addition of the term in Ω, which arises from the IEM mixing model. This term causes compositions $\boldsymbol{\phi}$ to relax to the mean $\widetilde{\boldsymbol{\phi}}$ at the rate Ω. However, approaching the DNS limit, there are no departures from the mean (i.e. $\boldsymbol{\phi} = \widetilde{\boldsymbol{\phi}}$, Equation 16) and hence the term is zero. Thus, in the approach to the DNS limit, the LES-PDF-MD equation admits the same solution as the DNS-PDF equation, and hence we conclude that the mean drift model is consistent and has the correct approach to the DNS limit, i.e. it behaves correctly.

   This important conclusion notwithstanding, we note that, approaching the DNS limit, the relaxation rate is

$$\Omega = C_m \frac{\widetilde{\mathcal{D}}}{\Delta^2} = \frac{C_m \widetilde{\mathcal{D}}}{\delta^2} \left(\frac{\Delta}{\delta} \right)^{-2}, \tag{25}$$

and hence tends to infinity. Thus, while the delta-function PDFs given as solutions to the DNS-PDF and MD-PDF equations are identical, the equations themselves are not. For this reason, our definitions of consistency and the correct approach are based on solutions, not on equations.

3.6. *The random-walk model in the DNS limit*

Compared to the DNS-PDF equation (Equation 18), the differences in the RW-PDF equation (Equation 11) in the DNS limit are the addition of the term in Ω stemming from the IEM model, and that the effects of molecular diffusion appear as a diffusion of the PDF (the first term on the right-hand side of Equation 11, with $\widetilde{\mathcal{D}}_e = \widetilde{\mathcal{D}}$ in the DNS limit) instead of as a drift in composition space. The effects of these differences are best revealed by examining the evolution equation for the residual covariance.

Looking first at the mean-drift model, the evolution equation for the residual covariance (deduced from Equation 15) is

$$\langle\rho\rangle\frac{\partial}{\partial t}\widetilde{\phi''_\alpha\phi''_\beta} + \langle\rho\rangle\mathbf{U}\cdot\nabla\widetilde{\phi''_\alpha\phi''_\beta} = \nabla\cdot(\langle\rho\rangle\widetilde{\mathcal{D}}_r\nabla\widetilde{\phi''_\alpha\phi''_\beta})$$
$$+ 2\langle\rho\rangle\widetilde{\mathcal{D}}_r\nabla\widetilde{\phi}_\alpha\cdot\nabla\widetilde{\phi}_\beta - 2\langle\rho\rangle\Omega\,\widetilde{\phi''_\alpha\phi''_\beta}$$
$$+ \langle\rho\rangle\widetilde{\phi''_\alpha S_\beta} + \langle\rho\rangle\widetilde{\phi''_\beta S_\alpha}. \qquad (26)$$

In the DNS limit, the residual covariance and $\widetilde{\mathcal{D}}_r$ are zero, and hence the right-hand side of this equation is zero. Thus there is no mechanism causing the residual covariance to depart from zero. This again shows that the mean-drift model approaches the DNS limit correctly, with the residual covariance being zero (independent of Δ/δ).

For the random-walk model, the residual covariance equation is almost the same, but with the effective diffusivity $\widetilde{\mathcal{D}}_e$ in place of the residual diffusivity $\widetilde{\mathcal{D}}_r$ in the first two terms on the right-hand side. But this difference is crucial, because, in the DNS limit, the second term on the right-hand side is then non-zero, and yields the *spurious production* term $2\langle\rho\rangle\widetilde{\mathcal{D}}\nabla\widetilde{\phi}_\alpha\cdot\nabla\widetilde{\phi}_\beta$. This spurious production causes the residual variances to depart from zero (at locations where there are non-zero composition gradients).

It may be expected, and is confirmed by the results presented below, the dominant balance in the residual-covariance equation is between the spurious production and relaxation term in Ω. A balance between these two terms yields

$$\widetilde{\phi''_\alpha\phi''_\beta} = \frac{\widetilde{\mathcal{D}}}{\Omega}\nabla\widetilde{\phi}_\alpha\cdot\nabla\widetilde{\phi}_\beta = \frac{\Delta^2}{C_m}\nabla\widetilde{\phi}_\alpha\cdot\nabla\widetilde{\phi}_\beta. \qquad (27)$$

This result shows that the random-walk model has an incorrect approach to the DNS limit, with residual fluctuations scaling with Δ. It is however consistent (as the residual covariance tends to zero, and the mean evolves by the correct equation).

It is interesting to observe that, with the random-walk model and the specification $C_m = 12$, the residual covariance given by Equation (27) is the same as that given by Equation (23). (We do not ascribe any significance to this observation.)

3.7. *Summary of the DNS limit*

To summarise the conclusion from this section: as the DNS limit is approached there are no residual fluctuations, the residual covariance is zero, and the PDF is a delta function, independent of Δ/δ (provided that it is sufficiently small to resolve the velocity field). Both the mean-drift and random-walk models are consistent with this limit. The mean-drift model approaches this limit correctly (e.g. with zero residual covariance); whereas, because of the spurious production of residual fluctuations, the random-walk model has an incorrect approach, with the residual covariance varying as $(\Delta/\delta)^2$.

4. Idealised, unstrained, plane, premixed laminar flame

4.1. *Definition of the test case*

The first test case we consider is that of an idealised, unstrained, one-dimensional, plane, premixed laminar flame. The single direction of variation is denoted by x. The chemistry is described by a single composition variable, $\phi(x, t)$, which may be considered to be a normalised product mass fraction, or a reaction progress variable. At $x = -\infty$ there are pure reactants ($\phi = 0$), and at $x = \infty$ there are completely burnt products ($\phi = 1$). In a frame fixed with the unburnt reactants, the flame propagates to the left at the flame speed u_F. Alternatively, in the frame fixed to the flame, the reactants flow to the right at speed u_F.

The very simple thermochemistry is defined in terms of ϕ as follows. The temperature T is specified as

$$T = T_u + \phi(T_b - T_u), \tag{28}$$

where T_u and T_b are the temperatures of the unburnt and burnt mixture. For definiteness, we take $T_u = 300$ K and $T_b = 2100$ K, although it is only the ratio $T_b/T_u = 7$ that is significant. Consistent with the ideal gas law, the density and specific volume are then specified as

$$\rho(T) = \rho_u \frac{T_u}{T}, \quad v(T) = v_u \frac{T}{T_u}, \tag{29}$$

where $\rho_u = 1/v_u$ are the unburnt values.

The molecular diffusivity is specified as

$$\mathcal{D}(T) = \mathcal{D}_u \left(\frac{T}{T_u}\right)^{1.72}, \tag{30}$$

which is based on an accurate approximation for methane combustion [17], with $\mathcal{D}_u$ being the unburnt value.

For each quantity introduced, the value in the burnt stream is denoted by ρ_b, v_b and $\mathcal{D}_b$. The density and specific volume ratios are 7 (like the temperature), while the diffusivity ratio is $\mathcal{D}_b/\mathcal{D}_u \approx 28$.

The chemical source term is specified to be

$$S(\phi) = \begin{cases} 0 & \text{for } \phi < \phi_R \\ \dfrac{1}{\tau_c}\dfrac{4}{27}z(1-z)^2 & \text{for } \phi \geq \phi_R, \end{cases} \tag{31}$$
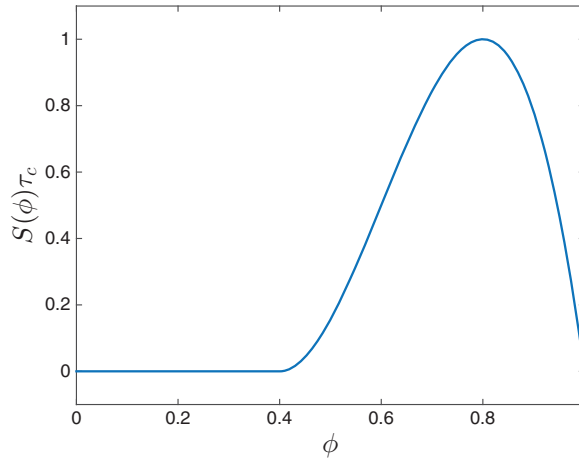
Figure 1.   Normalised reaction source term, Equation (31). (Colour online).

where τ_c is the chemical timescale, ϕ_R is taken to be 0.4, and z is defined by

$$z \equiv \frac{1 - \phi}{1 - \phi_R}. \tag{32}$$

The resulting normalised function $S(\phi)\tau_c$ is shown in Figure 1. The factor of 4/27 in Equation (31) is chosen to make the maximum value of $S(\phi)\tau_c$ unity.

For this simple 1D case, it is not necessary to consider the momentum equation, as the velocity is determined by mass conservation. Specifically, in the frame fixed with the flame, the mass flux is uniform, so that the velocity U is obtained from the relation

$$\rho\, U = \rho_u u_F. \tag{33}$$

We arbitrarily set ρ_u, $\mathcal{D}_u$ and τ_c to unity, and so all quantities obtained can be considered to be normalised by them.

4.2. *Solutions considered*

For this test case, we consider the following five solutions.

(1) The numerically-accurate solution of the governing equation (Equation 3), i.e. the laminar-flame solution; or, equivalently, the DNS solution.
(2) The numerically-accurate solution of the LES/PDF random-walk equations in the DNS limit.
(3) The numerically-accurate solution of the LES/PDF mean-drift equations in the DNS limit.
(4) The numerical solution of the LES/PDF random-walk equations in the DNS limit.
(5) The numerical solution of the LES/PDF mean-drift equations in the DNS limit.
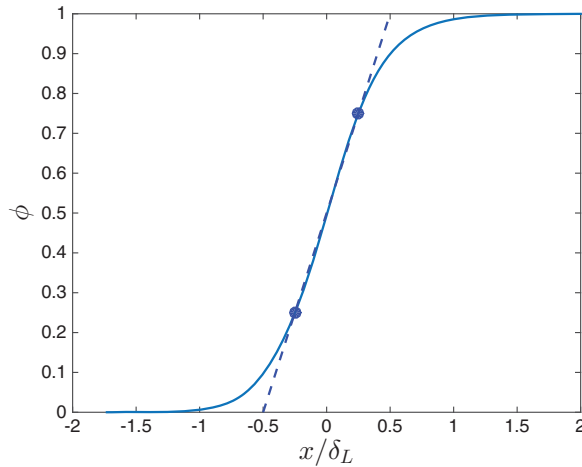
Figure 2.   Laminar flame profile. The symbols are the points on the profile where $\phi = [1/4\ \ 3/4]$, and the dashed line through them is the secant used to define the flame thickness. (Colour online).

4.3.   *DNS solution*

The laminar-flame or DNS solution is obtained by solving Equation (3) for the case considered by an accurate finite-difference method. The resulting composition profile is shown in Figure 2. In general, the flame speed is denoted by u_F and the flame thickness (defined below) is denoted by δ_F. However, for this reference, DNS solution, these quantities are denoted by s_L and δ_L, i.e. the laminar flame speed and thickness.

The measure of flame thickness we use is the *secant thickness*, defined as follows. Let $x_{1/4}$ and $x_{3/4}$ denote the locations at which the composition ϕ has the values 1/4 and 3/4, respectively. Then we define the thickness as

$$\delta_F = 2(x_{3/4} - x_{1/4}). \tag{34}$$

As illustrated in Figure 2, the geometric interpretation of this thickness is that it is the distance between the intersections of the secant through $x_{1/4}$ and $x_{3/4}$ and the pure stream values, $\phi = 0$ and $\phi = 1$. We use the secant thickness because it has the simple geometric interpretation given above, and because it can be extracted from numerical simulations more robustly than the gradient thickness. We also define the centre of the flame to be at the mid-point between $x_{1/4}$ and $x_{3/4}$. Thus, when the flame is centred at the origin ($x = 0$), it follows that $x_{1/4}/\delta_F = -1/4$ and $x_{3/4}/\delta_F = 1/4$.

The (normalised) laminar flame speed and thickness are found to be $s_L/(\mathcal{D}_u/\tau_c)^{1/2} = 0.81$ and $\delta_L/(\mathcal{D}_u\tau_c)^{1/2} = 7.6$.

4.4.   *Numerically-accurate solution for the mean-drift model*

As mentioned in Section 3.5, the numerically-accurate solution of the LES/PDF mean-drift model equations have the correct behaviour in the DNS limit. Thus the solution for $\widetilde{\phi}$ is just the laminar flame solution, and the variance of ϕ is zero. The value specified for the mixing rate Ω is immaterial.
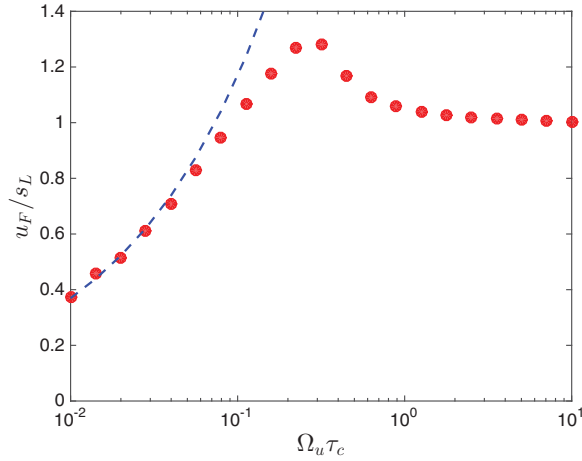
Figure 3. For the random-walk model, the normalised flame speed as a function of the normalised mixing rate. Dashed line: $3(\Omega_u\tau_c)^{1/2}$. (Colour online).
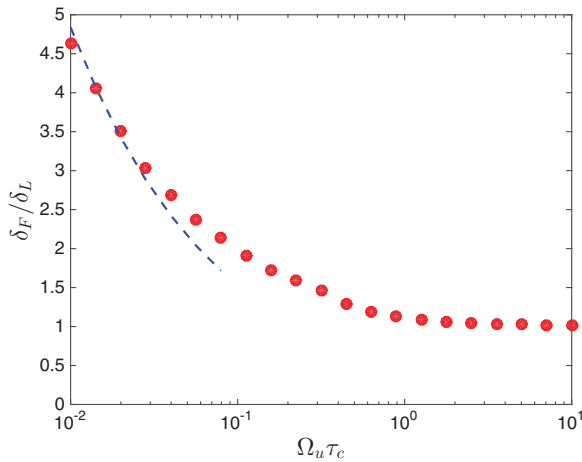

Figure 4. For the random-walk model, the normalised flame thickness as a function of the normalised mixing rate. Dashed line: $3.7(\Omega_u\tau_c)^{-1/2}$. (Colour online).

4.5. *Numerically-accurate solution for the random-walk model*

In contrast, the random-walk model does not have the correct behaviour in the DNS limit. In this case the solution depends on the specified (normalised) mixing rate $\Omega\tau_c$.

Numerically-accurate solutions for the random-walk model are obtained using the mesh-free particle method described in Appendix A. Consistent with Equation (10), the mixing rate is taken to be proportional to the molecular diffusivity, i.e.

$$\Omega = \Omega_u \frac{\mathcal{D}}{\mathcal{D}_u}, \qquad (35)$$

with the unburnt mixing rate, Ω_u, being a specified parameter.
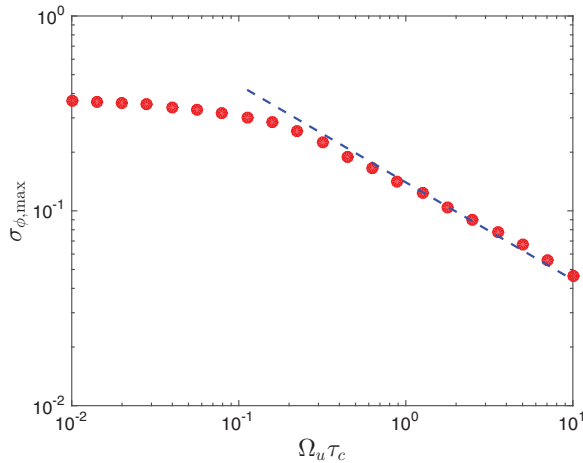
Figure 5. For the random-walk model, the maximum standard deviation of composition as a function of the normalised mixing rate. Dashed line: $0.14(\Omega_u\tau_c)^{-1/2}$. (Colour online).

The computed normalised flame speed and thickness are shown in Figures 3 and 4 as functions of the normalised unburnt mixing rate, $\Omega_u\tau_c$. As may be seen from these figures, as $\Omega_u\tau_c$ increases beyond unity, the flame speed and thickness become close to their laminar values.

Since the composition is non-reactive for $\phi < \phi_R = 0.4$, only by mixing does the composition rise from zero to ϕ_R. As a consequence, for small $\Omega_u\tau_c$, mixing is the rate-limiting process. If one assumes that (for small $\Omega_u\tau_c$) the flame speed and thickness are determined by $\mathcal{D}$ and Ω, independently of τ_c, then dimensional arguments dictate that u_F scales with $(\mathcal{D}_u\Omega_u)^{1/2}$, and that δ_F scales with $(\mathcal{D}_u/\Omega_u)^{1/2}$. As may be seen from Figures 3 and 4, the results for the four smallest values of $\Omega_u\tau_c$ investigated are consistent with these scalings.

It is interesting to observe that, as $\Omega_u\tau_c$ decreases, u_F/s_L first increases and attains a maximum of about 1.3 around $\Omega_u\tau_c \approx 0.3$, before decreasing, eventually with the mixing-limited scaling.

Figure 5 shows $\sigma_{\phi,\max}$, the maximum value (over all x) of the standard deviation of the composition. For small $\Omega_u\tau_c$, the standard deviation has the quite large value around 0.4, independent of τ_c. For large $\Omega_u\tau_c$, it decreases as $(\Omega_u\tau_c)^{-1/2}$, consistent with the balance of production and dissipation.

Figure 6 shows a scatter plot of particle composition through the flame. For the case shown ($\Omega_u\tau_c = 0.01$), mixing is rate limiting, and reaction in comparison is very fast. As a consequence, there are very few partially-burnt particles (i.e. $0.4 < \phi^* < 1$), and many fully-burnt particles (i.e. $\phi^* = 1$).

In summary, the numerically-accurate solution to the random-walk model in the DNS limit depends on the normalised mixing rate $\Omega_u\tau_c$. Because the residual variance is non-zero, the model behaves incorrectly in the DNS limit. However, for $\Omega_u\tau_c$ greater than unity, the flame speed and flame thickness are close to the laminar values, and the residual standard deviation is less than 10%. Consequently, in spite of the spurious residual variance, the random-walk model may be considered to be a useful and accurate model provided that the mixing rate is sufficiently large.
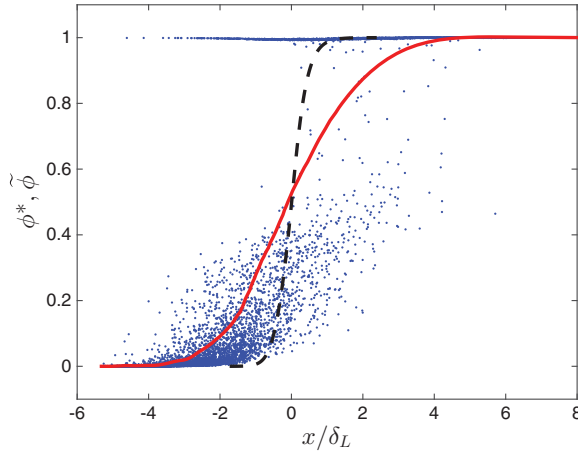
Figure 6. For the random-walk model with $\Omega_u \tau_c = 0.01$, a scatter plot of particle composition ϕ^* against position. Solid line: resolved composition $\widetilde{\phi}$. Dashed line: laminar flame profile. (Colour online).

4.6. *Cloud-in-cell solutions to the model equations*

In practice, the LES/PDF equations are not solved accurately (as considered in the previous subsection), but instead are solved by a numerical method that may incur significant error. This is because the mesh spacing h is typically chosen not to be very small compared to the resolution length scale Δ, and indeed may be larger than the smallest scale in the accurate solution to the LES/PDF equations (e.g. the flame thickness δ_F). We therefore consider here the numerical solution of the LES/PDF equations using the random-walk and mean-drift models obtained using a cloud-in-cell particle/mesh method. This is the type of method typically used in practice. The details of the current implementation are given in Appendix B.

For the given test case being considered, the numerical solution to the LES/PDF equations depends on three quantities: the specified resolution scale Δ, the specified mixing-model constant C_m, and the mesh spacing h. (We take the number of particles N to be large enough, and the time step Δt to be small enough, such that only the spatial discretisation error is significant.) It is convenient to reduce the number of parameters that need to be considered to two, which is possible since C_m and Δ enter solely through the combination C_m/Δ^2 (in Equation 10). To this end, we re-express the mixing rate as

$$\Omega = C_D \frac{\widetilde{\mathcal{D}}}{h^2}, \tag{36}$$

where comparison with Equation (10) shows that C_D and C_m are related by

$$C_D = C_m \left(\frac{h}{\Delta} \right)^2. \tag{37}$$

We then take the two parameters to be considered to be C_D and h/δ_L. Note that, for example, the value $C_D = 1$ corresponds both to $C_m = 1, h/\Delta = 1$, and to $C_m = 4, h/\Delta = 1/2$, etc.
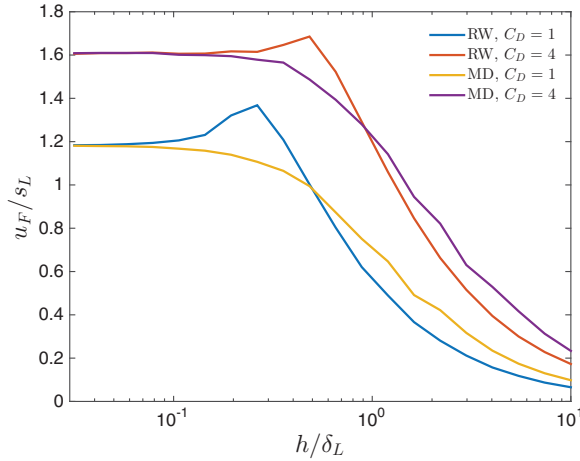
Figure 7. Using the cloud-in-cell method, the normalised flame speed as a function of the normalised mesh spacing for (from bottom to top at the right): the RW model with $C_D = 1$; the MD model with $C_D = 1$; the RW model with $C_D = 4$; the MD model with $C_D = 4$. (Colour online).

Figure 7 shows the computed flame speed as a function of the normalised mesh spacing for both models and for two values of the model coefficient C_D. For small h/δ_L both models attain the same asymptote, but with u_F/s_L being greater than unity, specifically 1.2 for $C_D = 1$ and 1.6 for $C_D = 4$. As with the accurate solution, with increasing mesh spacing, the flame speed of the random-walk model achieves a maximum, before decreasing. On the other hand the flame speed of the mean-drift model decreases monotonically, and is similar to that of the random walk model for large h/δ_L.

The key to understanding many of these observations is to appreciate that the CIC implementation of the IEM model incurs a numerical smearing error. A simple analysis shows that, to first order, this error is equivalent to there being an additional *numerical* diffusivity $\mathcal{D}_n$, which is proportional to Ωh^2. With α denoting the coefficient of proportionality, we have

$$\mathcal{D}_n = \alpha \Omega h^2 = \alpha C_D \widetilde{\mathcal{D}}. \tag{38}$$

Note that, for fixed C_D, this numerical diffusivity does not vanish as h/δ_L tends to zero, and it increases with C_D. This explains the observed values of u_F/s_L (for small h/δ_L) being greater than unity, and larger for $C_D = 4$ than for $C_D = 1$. (Below, we empirically determine the value $\alpha = 0.4$.)

This reasoning can be made quantitative as follows. We define the *augmented* diffusivity to be

$$\mathcal{D}_a \equiv \widetilde{\mathcal{D}} + \mathcal{D}_n = \widetilde{\mathcal{D}}(1 + \alpha C_D). \tag{39}$$

Just as the laminar flame speed and thickness scale as $(\mathcal{D}_u/\tau_c)^{1/2}$ and $(\mathcal{D}_u \tau_c)^{1/2}$, respectively, the numerical flame speed and thickness can be expected to scale as $(\mathcal{D}_a/\tau_c)^{1/2}$ and
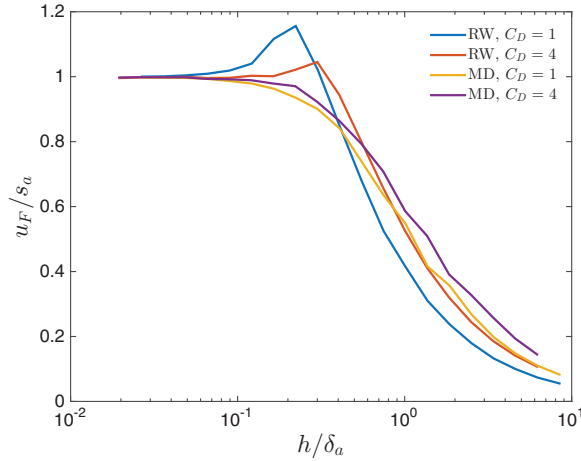
Figure 8. Using the cloud-in-cell method, the flame speed normalised by s_a as a function of the mesh spacing normalised by δ_a for (from bottom to top at the right): the RW model with $C_D = 1$; the RW model with $C_D = 4$; the MD model with $C_D = 1$; the MD model with $C_D = 4$. (Colour online).

$(\mathcal{D}_a \tau_c)^{1/2}$, respectively, and hence to be larger than the laminar values by a factor of

$$\left(\frac{\mathcal{D}_a}{\mathcal{D}_u} \right)^{1/2} = (1 + \alpha C_D)^{1/2}. \tag{40}$$

We thus define the *augmented* laminar flame speed and thickness to be

$$s_a \equiv (1 + \alpha C_D)^{1/2} s_L, \tag{41}$$

and

$$\delta_a \equiv (1 + \alpha C_D)^{1/2} \delta_L, \tag{42}$$

and, in Figure 8, we re-plot the computed flame speeds, but now with normalisation by s_a and δ_a. As may be seen, with the empirically-determined value of $\alpha = 0.4$, this scaling is successful in accurately yielding $u_F = s_a$ for small h/δ_a for all four cases.

Figure 9 shows the computed flame thicknesses normalised by δ_a. As may be seen, in all four cases, δ_F converges to δ_a as the mesh is refined. For large h, the flame thickness scales essentially with h, with $\delta_F \approx 4h$ for the random-walk model with $C_D = 1$, and $\delta_F \approx h$ for the mean-drift model with $C_D = 4$.

In the above we consider C_D to be a fixed parameter. If instead we revert to considering C_m to be fixed, then from Equation (41) we obtain (for small h/δ_L and h/Δ)

$$\frac{s_a}{s_L} = \left(1 + \alpha C_m \left[\frac{h}{\Delta} \right]^2 \right)^{1/2}$$

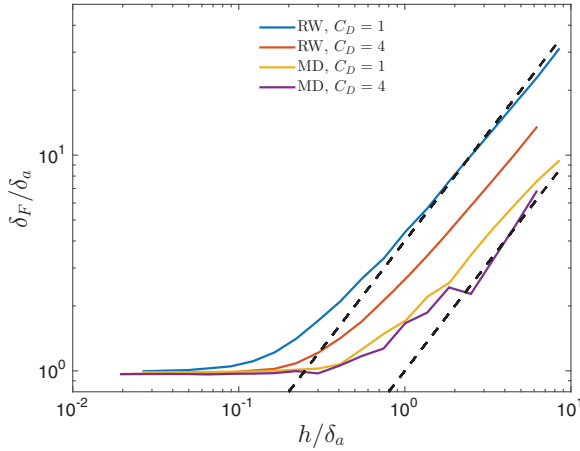$$\approx 1 + \frac{1}{2} \alpha C_m \left[\frac{h}{\Delta} \right]^2, \tag{43}$$

Figure 9. Using the cloud-in-cell method, the flame thickness as a function of the mesh spacing, both normalised by δ_a for (from bottom to top at the right): MD model, $C_D = 4$; MD model, $C_D = 1$; RW model, $C_D = 4$; RW model, $C_D = 1$. The lower and upper dashed lines are $\delta_F = h$ and $\delta_F = 4h$, respectively. (Colour online).

and similarly for δ_a/δ_L. The important conclusions are that, for fixed C_m, the correct laminar flame speed and thickness are obtained as the grid spacing h/δ_L tends to zero when Δ/δ_L is fixed, but not when h/Δ is fixed.

The last result – that the correct solution is not obtained in the limit $\Delta/\delta_L \to 0$, $h/\delta_L \to 0$, for fixed h/Δ – is perhaps surprising and deserves further comment.

Consider first the numerical solution of the implied equation (Equation 12) for the re-solved mean composition $\widetilde{\boldsymbol{\phi}}$ in which the residual diffusivity $\widetilde{\mathcal{D}}_r$ is given by the Smagorinsky model instead of being taken to be zero. In this case, compared to the DNS equation for composition (Equation 3), the implied equation for the mean composition contains a spurious diffusion term of order $(\Delta/\delta_L)^2$. Even if a numerical error of order one relative magnitude is incurred (e.g. by using the coarse mesh $h/\Delta = 1$), since the term itself vanishes in the limit $\Delta/\delta_L \to 0$, the numerical error does not prevent the solution from converging to the DNS solution.

Returning to the CIC solutions of the PDF equations, the fundamental reason that they do not converge to the DNS solutions (for fixed h/Δ) is that (as previously observed) the LES-PDF equations do not converge to the DNS-PDF equation: the IEM model introduces the term in Ω which, far from vanishing, in fact tends to infinity in the limit $\Delta/\delta_L \to 0$.

4.7. *Matching the laminar flame speed*

It is natural to ask: With the CIC implementation of the LES/PDF models, is it possible to specify the mixing rate Ω so that the flame speed u_F matches the laminar flame speed s_L, even if the mesh size h is not small compared to the laminar flame thickness δ_L? The answer is: Yes.

First consider the case when h/δ_L is large. In this case: the numerical diffusion $\mathcal{D}_n = \alpha \Omega h^2$ dominates the molecular diffusion; the flame thickness scales with h (see Figure 9); and the reaction is not rate limiting. Hence the flame speed is determined dominantly by $\mathcal{D}_n$ and h, with $\mathcal{D}$ and τ_c not being significant. It follows (on dimensional grounds) that the flame speed scales as $h\Omega$, and hence, to match the laminar flame speed (which scales
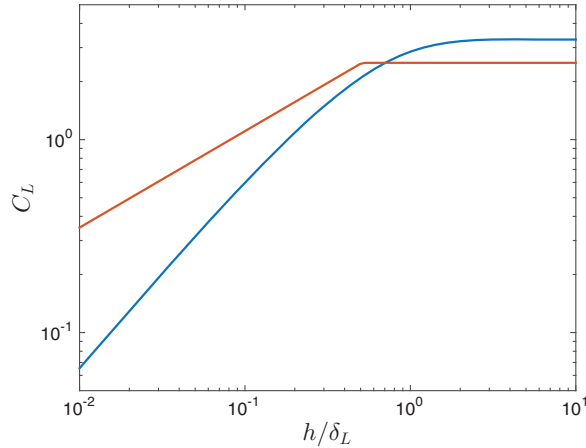
Figure 10.   Empirical coefficients $C_L(h/\delta_L)$ (Equations 45 and 46) yielding flame speeds equal to the laminar flame speed for the CIC implementation of the random-walk model (lower curve at left) and of the mean-drift model (upper curve at left). (Colour online).

as $\mathcal{D}/\delta_L$), Ω has to be specified to scale as $\mathcal{D}/(h\delta_L)$. Thus, for large h/δ_L, the appropriate specification is

$$\Omega = C_L \frac{\widetilde{\mathcal{D}}}{h\delta_L}, \tag{44}$$

where C_L is a constant. More generally, we can consider C_L to be a coefficient dependent on h/δ_L, which tends to a constant for large h/δ_L.

Before proceeding, we make the following observation based on the flame speed scaling with Ωh for large h/δ_L. It follows from Equation (44) that, by construction, for fixed C_L, u_F/s_L is independent of h/δ_L. It further follows from the relations between C_L, C_D and C_m that u_F/s_L varies as $(h/\delta_L)^{-1}$ for fixed C_D, and as $h\delta_L/\Delta^2 = (h/\Delta)^2(h/\delta_L)^{-1}$ for fixed C_m.

We determine empirically that the function $C_L(h/\delta_L)$ which yields $u_F = s_L$ is well approximated for the random-walk model by

$$C_L = 3.3 \left[1 - \exp\left(-2\frac{h}{\delta_L} \right) \right], \tag{45}$$

and for the mean-drift model by

$$C_L = \min\left(2.5,\ 3.5 \left[\frac{h}{\delta_L} \right]^{1/2} \right). \tag{46}$$

These functions are shown in Figure 10.

Note that, with everything except h fixed: for fixed C_D, Ω varies as h^{-2}; for large h/δ_L the above expressions for C_L imply that Ω varies as h^{-1}; while for small h/δ_L, C_L for the RW model (Equation 45) implies that Ω varies as h^0, whereas C_L for the MD model (Equation 46) implies that Ω varies as $h^{-1/2}$.
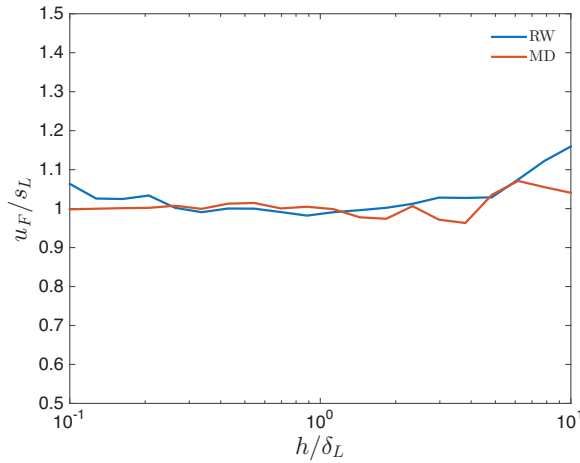
Figure 11. Normalised flame speed against normalised mesh spacing for the CIC implementations of the random-walk and mean-drift models with the mixing rate specified by Equations (44)–(46). (Colour online).
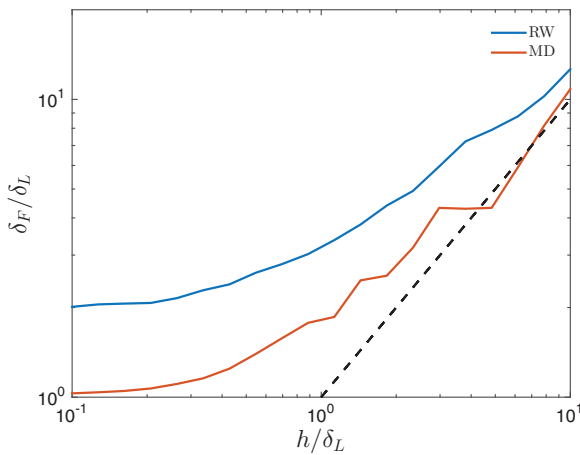

Figure 12. Normalised flame thickness against normalised mesh spacing for the CIC implementations of the random-walk model using Equation (45) (upper curve) and the mean-drift model using Equation (46) (lower curve). The dashed line is $\delta_F = h$. (Colour online).

The computed flame speeds using Ω given by Equations (44)–(46) are shown in Figure 11. As may be seen, with these specifications of C_L, both models do indeed yield flame speeds close to the laminar flame speed.

While both models yield the same flame speed, their solutions are quite different. While the mean-drift model is consistent with the DNS limit in producing no residual fluctuations, the random-walk model has large residual fluctuations (around 30%), even for small h/δ_L. This is because, for the RW model with C_L given by Equation (45), as h/δ_L tends to zero, Ω tends to the value $6.6\widetilde{\mathcal{D}}/\delta_L^2$, independent of h; whereas, in order to suppress residual fluctuations and hence to reproduce the DNS limit, Ω must vary as a negative power of h/δ_L (as it does for a fixed value of C_D).

As a further manifestation of the differences between the model solutions, Figure 12 shows the normalised flame thicknesses. For small h/δ_L, the mean-drift model correctly yields $\delta_F = \delta_L$; and for large h/δ_L it yields $\delta_F \approx h$. In contrast, the random-walk model yields consistently thicker flames, with $\delta_F \approx 2\delta_L$ for small h/δ_L.

We conclude this subsection with the following caveats and reservations. A great virtue of PDF methods is that they are generally applicable to all modes and regimes of combustion. However, the specification of the mixing rate Ω by Equations (44)–(46) is anything but general. It is particular to homogeneously-premixed combustion, so that a unique laminar flame thickness δ_L can be defined. Furthermore, the appropriate specification of the coefficient C_L depends on the details of the numerical implementation.

5. Strained methane/air premixed laminar flame

5.1. *Definition of the test case*

The flow considered consists of two opposed round jets emanating from nozzles of diameter $D = 12.7$ mm placed at a distance of $d = 16$ mm apart. One of the nozzles emits a fresh (unburnt) mixture of $CH_4/O_2/N_2$ at equivalence ratio $\phi_u = 0.85$ ($O_2/N_2 = 30/70$ molar ratio), temperature $T_u = 294$ K and pressure 1 atm. The other nozzle emits fully-burnt combustion products at temperature $T_{ad} = 2435$ K, corresponding to the chemical-equilibrium mixture with the same enthalpy, elemental composition and pressure as the reactant stream. The axial velocity of the reactant stream is $U_u = 1$ m/s, and that of the product stream is taken to be twice this value so that the resulting laminar flame is approximately mid-way between the nozzles. The nominal mean strain rate is thus $2U_u/d = 125s^{-1}$. The radial velocities at the nozzle exits are taken to be zero.

The axial coordinate is denoted by z, with $z = -8$ mm being the product-stream nozzle exit, and $z = 8$ mm being the reactant-stream nozzle exit.

The methane combustion is described by a 16-species augmented reduced mechanism for methane oxidation [27]. The thermal diffusivity is obtained from the CHEMKIN transport library, and then the (equal) species diffusivities are obtained by taking the Lewis numbers to be unity.

5.2. *OPPDIF calculations*

As is well known [28], for the flow considered, the profiles along the centreline can be obtained from the solution of 1D equations. These equations are solved using the OPPDIF code within CHEMKIN-PRO [22]. Figure 13(a) shows the computed axial profiles of the axial velocity and temperature. Figure 13(b) shows the profile of $\rho U/\rho_u$. The value of the laminar flame speed s_L is taken to be the value of $\rho U/\rho_u$ at the location of maximum temperature gradient. This location is around $z = 4$ mm, and the resulting value of s_L is 55.8 cm/s. The secant thickness (obtained from the normalised temperature profile ($T - T_u$)/($T_{ad} - T_u$) and Equation (34)) is $\delta_L = 0.334$ mm.

5.3. *LES/PDF calculations*

LES/PDF calculations are performed in the DNS limit using the coupled NGA/HPDF code [6,29,30]. The number of grid points in the radial and azimuthal directions are kept constant at 48 and 4 respectively, while the number of grid points in the axial direction, n_x, is varied from 12 to 384 in order to span the range of values of Δ/δ_L typically used in
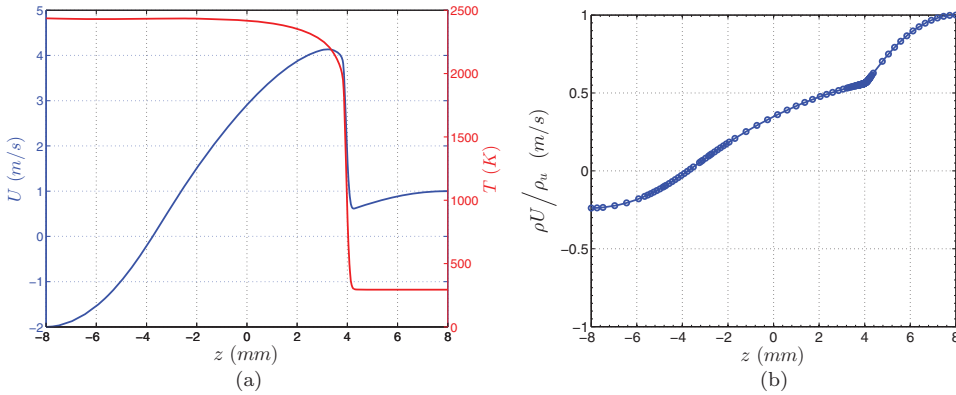
Figure 13.   Laminar profiles from the OPPDIF calculations of (a) velocity and temperature and (b) $\rho U/\rho_u$ as a function of axial coordinate between the two nozzles. (Colour online).
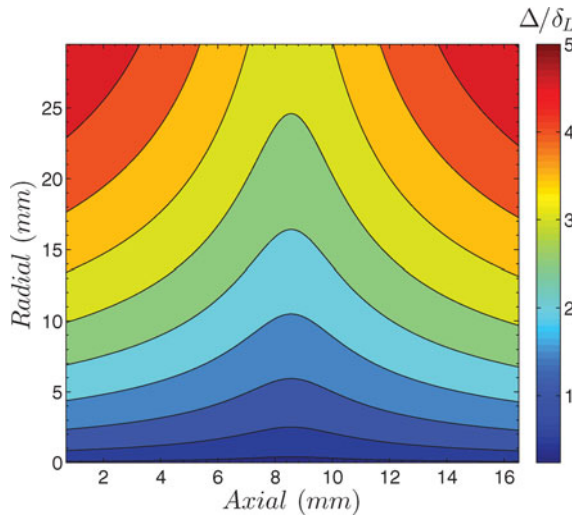

Figure 14.   Contour plot of normalised filter-width from the previous 3D LES/PDF simulations of turbulent premixed counterflow flames described in [10]. (Colour online).

LES/PDF calculations. To illustrate this range, Figure 14 shows a contour plot of the values of Δ/δ_L observed in recent 3D LES/PDF simulations of turbulent premixed counterflow flame [10]. Note that the filter-width in the present simulations is taken to be equal to the (uniform) grid spacing in the axial direction, i.e. $\Delta = h$.

   The results reported below depend on: the model used (random walk or mean drift); the value of the mixing-rate constant C_m; and the specified axial grid spacing and resolution length scale $h = \Delta$. The values of C_m used are 1.0 and 4.0. By using different grids, h/δ_L is varied between 0.13 and 4.0.

5.4.   *Results*

Figures 15 and 17 show the normalised flame speed and flame thickness as functions of the normalised grid spacing for both models and for both values of C_m investigated. The
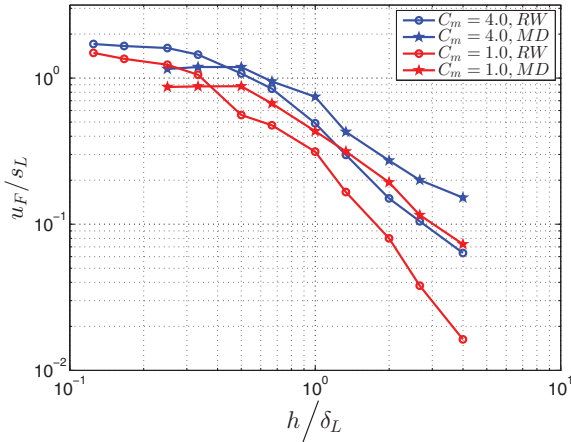
Figure 15. Normalised flame speed as a function of normalised grid spacing for: $C_m = 4.0$, RW (blue dot); $C_m = 4.0$, MD (blue star); $C_m = 1.0$, RW (red dot); $C_m = 1.0$, MD (red star). (The curves for $C_m = 1.0$ are below the corresponding curves for $C_m = 4.0$.) (Colour online).

flame speed u_F and the flame thickness δ_F are obtained from the centreline profiles of the resolved velocity, density and temperature in the same way as for the OPPDIF calculations (as described in Section 5.2).

For the flame speed, the observed behaviour (Figure 15) is broadly the same as for the CIC solution for the idealised, unstrained 1D flame considered in Section 4.6 (see Figure 7). For the random-walk model, u_F/s_L has an asymptote, larger than unity, for small h/δ_L, and then decreases with increasing h/δ_L. The values of u_F/s_L for $C_m = 4$ are consistently higher than those for $C_m = 1$. The only qualitative difference compared to the results in Figure 7 is that a local maximum in u_F/s_L around $h/\delta_L \approx 0.4$ is not observed.

For the mean-drift model, the results are qualitatively similar. The only point of note is that, for $C_m = 1$, the asymptotic value of u_F/s_L is about 0.9, i.e. less than unity. Further investigation reveals that this is due to time-stepping error. As shown in Figure 16, as the time step decreases, u_F/s_L increases, plausibly exceeding unity for smaller time steps than investigated.

Figure 17 shows the normalised flame thickness as a function of the normalised grid spacing. The observations are the same as for the CIC solutions for the idealised, unstrained flame (see Figure 9). The flame thickness is generally larger for the random-walk model than for the mean-drift model, and decreases with increasing C_m. On the finest grids, δ_F/δ_L approaches an asymptote greater than unity; while on coarse grids the flame thickness is approximately $\delta_F \approx 2.5h$ (in three out of the four cases).

Figure 18 shows scatter plots on the centreline of the particle temperature versus position, colour coded by the mass fraction of OH. The left-hand column is for the random-walk model, and the right-hand column for the mean-drift model. The top two rows are for $C_m = 4$, and the bottom two for $C_m = 1$. The first and third rows are for the relatively coarse grid ($h/\delta = 1.4$), while the second and fourth rows are for the finer grid ($h/\delta = 0.5$). The symbols on the top axis of each plot show the locations of the grid nodes.

The first observation to be made from these scatter plots is that the implementation of the mean-drift model is successful in producing negligible residual fluctuations in all cases. It may also be observed that the particles are, to some extent, able to resolve the
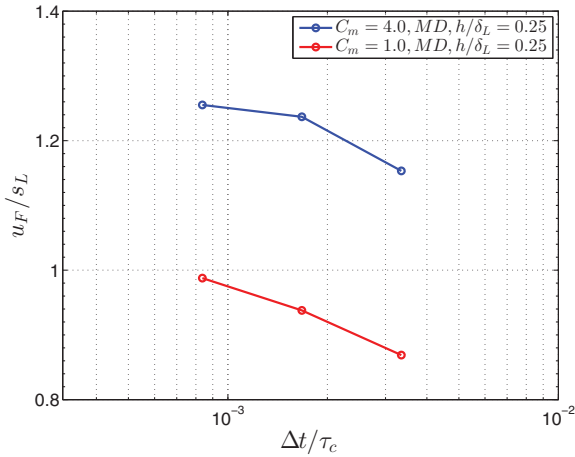
Figure 16. Normalised flame speed as a function of normalised time step for $C_m = 4.0$, MD, $h/\delta_L = 0.25$ (upper curve) and $C_m = 1.0$, MD, $h/\delta_L = 0.25$ (lower curve). Here, τ_c is defined by $\tau_c \equiv \delta_L/s_L$. (Colour online).
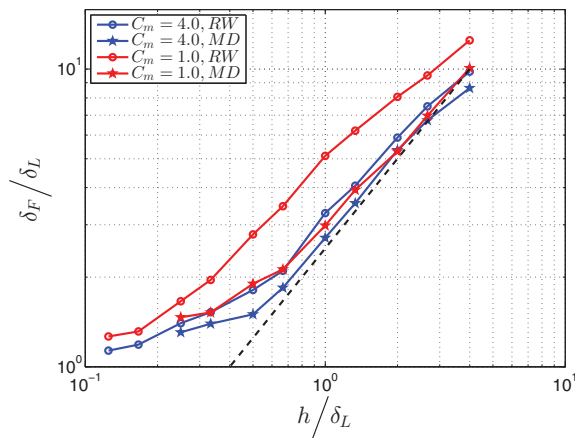

Figure 17. Normalised flame thickness as a function of normalised grid spacing for: $C_m = 4.0$, RW (blue dot); $C_m = 4.0$, MD (blue star); $C_m = 1.0$, RW (red dot); $C_m = 1.0$, MD (red star). The dashed line is $\delta_F = 2.5h$. (The curves for $C_m = 1.0$ are above the corresponding curves for $C_m = 4.0$.) (Colour online).

flame profile below the grid scale. For the random-walk model there is appreciable scatter (inconsistent with the DNS limit), which decreases with increasing C_m and with decreasing h/δ_L.

The results presented in this section serve to confirm the validity of the model implementations in the 3D LES/PDF code in the DNS limit. They also confirm that the results obtained for the idealised, unstrained flame using the 1D MATLAB® script are representative of those obtained with the much more complex 3D LES/PDF code.
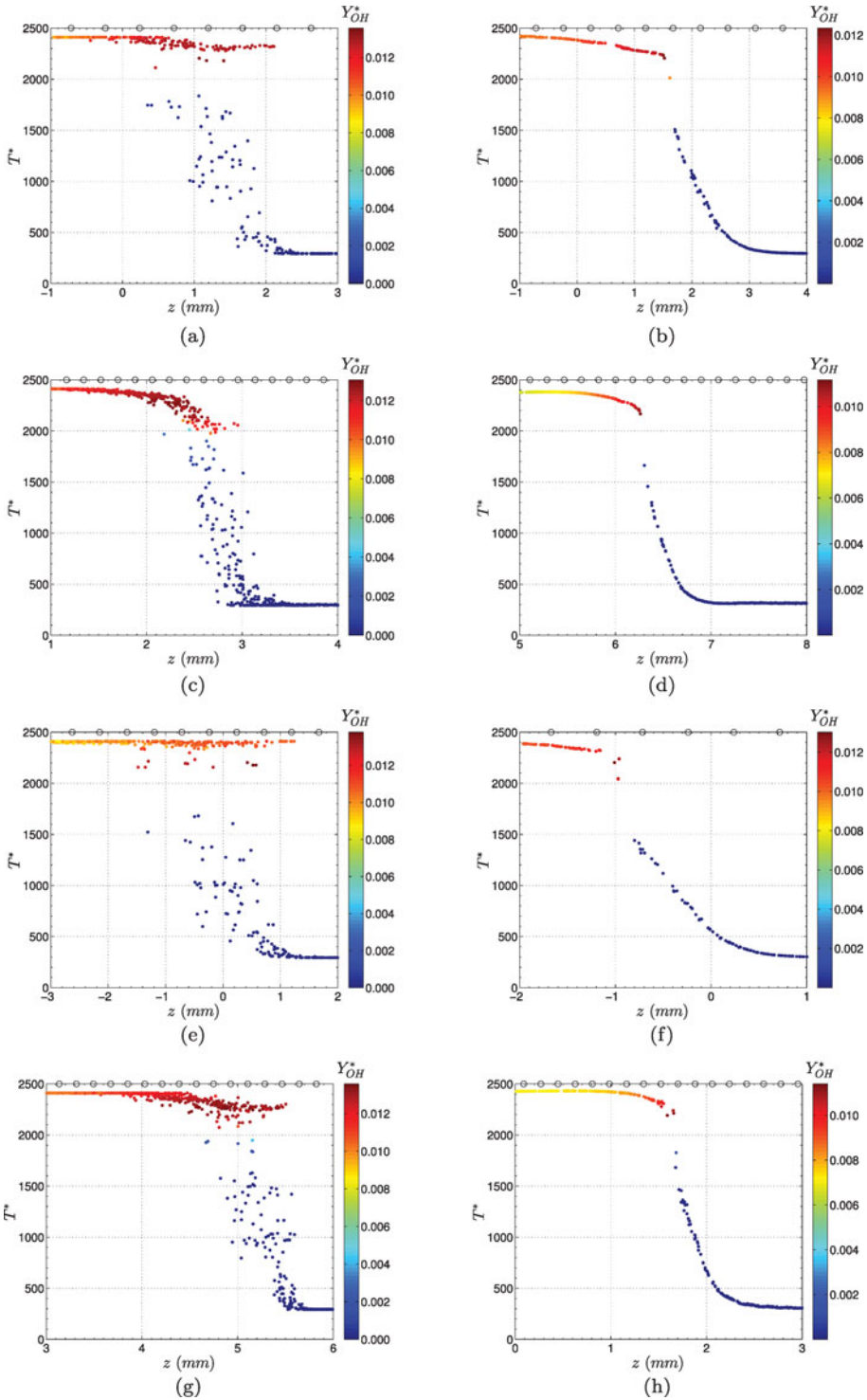
Figure 18.   Scatter plots of particle temperature on the centreline colour coded by particle OH species mass fraction for (a) $C_m = 4.0$, RW, $h/\delta_L = 1.4$, (b) $C_m = 4.0$, MD, $h/\delta_L = 1.4$, (c) $C_m = 4.0$, RW, $h/\delta_L = 0.5$, (d) $C_m = 4.0$, MD, $h/\delta_L = 0.5$, (e) $C_m = 1.0$, RW, $h/\delta_L = 1.4$, (f) $C_m = 1.0$, MD, $h/\delta_L = 1.4$, (g) $C_m = 1.0$, RW, $h/\delta_L = 0.5$, (h) $C_m = 1.0$, MD, $h/\delta_L = 0.5$. The grid points are shown as black circles at the top of the figures. (Colour online).

6. Discussion

Based on the results presented above and other considerations, it is clear that the mean-drift model has significant theoretical advantages over the random-walk model. These advantages are as follows.

(1) Differential diffusion can be implemented in the mean-drift model, whereas with the random-walk model the unity-Lewis-number assumption is unavoidable.
(2) The mean-drift model behaves correctly in the DNS limit, whereas the random-walk model has spurious production of variance leading to significant residual fluctuations.
(3) In the CIC implementation of the models, on a given mesh, the flame thickness δ_F given by the mean-drift model is significantly smaller (i.e. closer to δ_L) than that given by the random-walk model.

However, the mean-drift model also has distinct disadvantages in ease of implementation and computational cost. Specifically:

(i) with the mean-drift model, special measures must be taken to guarantee realizability (e.g. imposing a lower limit on the mixing rate to ensure that species mass fractions remain non-negative [25,26]);
(ii) the mean-drift model requires the evaluation of the n_ϕ resolved composition fields $\widetilde{\boldsymbol{\phi}}(\mathbf{x}, t)$ (which is computationally expensive) and the solution of n_ϕ PDEs to determine the mean drift.

In contrast, the random-walk model can be implemented in an efficient, mesh-free algorithm that automatically guarantees realizability and does not require the evaluation of the resolved compositions. Because of these practical advantages, and in spite of its theoretical disadvantages, we do not advocate abandoning the random-walk model: it may be adequate (and simpler and cheaper) for a range of problems in which differential diffusion and consistency with the DNS limit are not crucial.

7. Conclusions

The principal conclusions to be drawn from this work are as follows.

(1) In considering LES in the DNS limit, it is advantageous to define the resolved quantities as conditional means rather than as filtered fields. With the conditional-mean approach, in the DNS limit, the resolved fields in LES are just the DNS fields, and there are no residual fluctuations. In contrast, with the filtering approach, the resolved fields differ from the DNS fields (by of order $(\Delta/\delta)^2$), and the residual variances are non-zero (and are, again, of order $(\Delta/\delta)^2$).
(2) An LES method is said to be consistent in the DNS limit if the numerical solution of the LES equations converges to the solution of the DNS equations in the limit $\Delta/\delta \to 0$ and $h/\delta \to 0$ (possibly with additional requirements on the ratio h/Δ).
(3) An LES method is said to behave correctly in the DNS limit if it is consistent and it approaches the limit correctly. For the LES-PDF equations applied to laminar flames, the correct behaviour is that the residual composition fluctuations are zero, independently of Δ/δ_L.

(4) The behaviour of LES/PDF models in the DNS limit has been studied by applying them to two laminar premixed flames: an idealised unstrained flame, and a strained methane/air flame.

(5) The numerically-accurate solutions to the LES/PDF equations incorporating the mean-drift model exhibit the correct behaviour in the DNS limit.

(6) A mesh-free particle method has been implemented to obtain numerically-accurate solutions to the LES/PDF equation incorporating the random-walk model (i.e. the RW-PDF equation).

(7) These numerically-accurate solutions to the RW-PDF equation exhibit an incorrect behaviour in the DNS limit, in that the residual fluctuations are non-zero. However, if the mixing rate Ω is sufficiently large (e.g. $\Omega \tau_c \gtrsim 1$), then the flame speed and thickness are close to the laminar values, and the residual fluctuations are not large (e.g. less than 10%).

(8) The cloud-in-cell implementation of the IEM mixing model incurs a smearing error which is equivalent to a numerical diffusion $\mathcal{D}_n$ that scales as Ωh^2.

(9) With the standard specification of the mixing rate, with a constant value of C_m, as the mesh is refined (i.e. $h/\delta_L \to 0$), the LES/PDF solutions are consistent with the DNS limit if the resolution scale is fixed (i.e. Δ/δ_L is fixed), but not if h/Δ is fixed.

(10) On coarse meshes ($h/\delta_L \gg 1$): the flame thickness δ_F scales with the mesh spacing h; the mixing rate Ω and the mesh spacing h are the controlling parameters (with the molecular diffusivity $\mathcal{D}$ and the reaction timescale τ_c not being controlling); and hence the flame speed u_F scales as Ωh.

(11) On coarse meshes, and with C_m and h/Δ fixed, the normalised flame speed u_F/s_L scales with $(h/\delta_L)^{-1}$.

(12) With both the RW and the MD model, it is possible to specify the mixing rate (by Equations 44–46) so that the flame speed u_F matches the laminar flame speed s_L, even on coarse meshes. It is emphasised that this is a non-general model.

(13) Computations have been performed of a strained, premixed, methane/air, opposed-jet flame, using the same 3D code used in previous LES/PDF studies. The results confirm the validity of the model implementations in the 3D code in the DNS limit; and they confirm that the results obtained for the idealised, unstrained flame are representative of those obtained with the much more complex 3D LES/PDF code.

(14) Whereas the mean-drift model has theoretical advantages (in allowing differential diffusion to be implemented and behaving correctly in the DNS limit), the random-walk model has the practical advantages of being simpler to implement and being computationally less expensive.

Disclosure statement

No potential conflict of interest was reported by the authors.

References

[1] S.B. Pope, *PDF methods for turbulent reactive flows*, Prog. Energy Combust. Sci. 11 (1985), pp. 119–192.

[2] D.C. Haworth, *Progress in probability density function methods for turbulent reacting flows*, Prog. Energy Combust. Sci. 36 (2010), pp. 168–259.

[3] S.B. Pope, *Small scales, many species and the manifold challenges of turbulent combustion*, Proc. Combust. Inst. 34 (2013), pp. 1–31.

[4] F.A. Jaberi, P.J. Colucci, S. James, P. Givi and S.B. Pope, *Filtered mass density function for large-eddy simulation of turbulent reacting flows*, J. Fluid Mech. 401 (1999), pp. 85–121.

[5] V. Raman and H. Pitsch, *A consistent LES/filtered-density function formulation for the simulation of turbulent flames with detailed chemistry*, Proc. Combust. Inst. 31 (2007), pp. 1711–1719.

[6] Y. Yang, H. Wang, S.B. Pope and J.H. Chen, *Large-eddy simulation/probability density function modeling of a non-premixed CO/H_2 temporally evolving jet flame*, Proc. Combust. Inst. 34 (2013), pp. 1241–1249.

[7] I.A. Dodoulas and S. Navarro-Martinez, *Large eddy simulation of premixed turbulent flames using the probability density function approach*, Flow Turbul. Combust. 90 (2013), pp. 645–678. Available at http://dx.doi.org/10.1007/s10494-013-9446-z.

[8] J. Kim and S.B. Pope, *Effects of combined dimension reduction and tabulation on the simulations of a turbulent premixed flame using large-eddy simulation/probability density function*, Combust. Theory Model. 18 (2014), pp. 388–413.

[9] S.B. Pope and R. Tirunagari, *Advances in probability density function methods for turbulent reactive flows*, in *Proceedings of the Nineteenth Australasian Fluid Mechanics Conference*, RMIT University, Melbourne, 2014.

[10] R.R. Tirunagari and S.B. Pope, *An investigation of turbulent premixed counterflow flames using large-eddy simulations and probability density function methods*, Combust. Flame 166 (2016), pp. 229–242.

[11] S.B. Pope, *Turbulent Flows*, Cambridge University Press, Cambridge, UK, 2000.

[12] H. Pitsch, *Large-eddy simulation of turbulent combustion*, Annu. Rev. Fluid. Mech. 38 (2006), pp. 453–482.

[13] S.B. Pope, *Self-conditioned fields for large-eddy simulations of turbulent flows*, J. Fluid Mech. 652 (2010), pp. 139–169.

[14] R.S. Rogallo and P. Moin, *Numerical simulation of turbulent flows*, Annu. Rev. Fluid. Mech. 17 (1985), pp. 99–137.

[15] R.O. Fox, *Computational Models for Turbulent Reactive Flows*, Cambridge University Press, New York, 2003.

[16] S.B. Pope, *Ten questions concerning the large-eddy simulation of turbulent flows*, New J. Phys. 6 (2004), Article No. 35. Available at http://dx.doi.org/10.1088/1367-2630/6/1/035.

[17] K.A. Kemenov and S.B. Pope, *Molecular diffusion effects in LES of a piloted methane–air flame*, Combust. Flame 157 (2011), pp. 240–254.

[18] R.S. Barlow and J.H. Frank, *Effects of turbulence on species mass fraction in methane/air jet flames*, Proc. Combust. Inst. 27 (1998), pp. 1087–1095.

[19] O.T. Stein, B. Boehm, A. Dreizler and A.M. Kempf, *Highly-resolved LES and PIV analysis of isothermal turbulent opposed jets for combustion applications*, Flow Turbul. Combust. 87 (2011), pp. 425–447.

[20] A.M. Ruiz, G. Lacaze and J.C. Oefelein, *Flow topologies and turbulence scales in a jet-in-cross-flow*, Phys. Fluids 27 (2015), Article ID 045101. Available at http://dx.doi.org/10.1063/1.4915065.

[21] J. Villermaux and J.C. Devillon, *Représentation de la coalescence et de la redispersion des domaines de ségrégation dans un fluide par un modèle d'interaction phénoménologique*, in *Proceedings of the 2nd International Symposium on Chemical Reaction Engineering*, 2–4 May 1972, Amsterdam. Elsevier, New York, 1972, pp. B1–B13.

[22] R.J. Kee, F.M. Rupley, J.A. Miller, M.E. Coltrin, J.F. Grcar, E. Meeks, H.K. Moffat, A.E. Lutz, G. Dixon-Lewis, M.D. Smooke, J. Warnatz, G.H. Evans, R.S. Larson, R.E. Mitchell, L.R. Petzold, W.C. Reynolds, M. Caracotsios, W.E. Stewart, P. Glarborg, C. Wang and O. Adigun, *CHEMKIN Collection, Release 3.6*, Reaction Design, San Diego, CA, 2000.

[23] S.B. Pope, *Computations of turbulent combustion: progress and challenges*, Proc. Combust. Inst. 23 (1990), pp. 591–612.

[24] P.J. Colucci, F.A. Jaberi, P. Givi and S.B. Pope, *Filtered density function for large eddy simulation of turbulent reacting flows*, Phys. Fluids 10 (1998), pp. 499–515.

[25] R. McDermott and S.B. Pope, *A particle formulation for treating differential diffusion in filtered density function methods*, J. Comput. Phys. 226 (2007), pp. 947–993.

[26] S. Viswanathan, H. Wang and S.B. Pope, *Numerical implementation of mixing and molecular transport in LES/PDF studies of turbulent reacting flows*, J. Comput. Phys. 230 (2011), pp. 6916–6957.

[27] C.J. Sung, C.K. Law and J.Y. Chen, *An augmented reduced mechanism for methane oxidation with comprehensive global parametric validation*, Proc. Combust. Inst. 27 (1998), pp. 295–304.

[28] R.J. Kee, M.E. Coltrin and P. Glarborg, *Chemically Reacting Flow: Theory and Practice*, Wiley, Hoboken, NJ, 2003.

[29] O. Desjardins, G. Blanquart, G. Balarac and H. Pitsch, *High order conservative finite difference scheme for variable density low Mach number turbulent flows*, J. Comput. Phys. 227 (2008), pp. 7125–7159.

[30] H. Wang and S.B. Pope, *Large eddy simulation/probability density function modeling of a turbulent $CH_4/H_2/N_2$ jet flame*, Proc. Combust. Inst. 33 (2011), pp. 1319–1330.

[31] S.B. Pope, *A model for turbulent mixing based on shadow-position conditioning*, Phys. Fluids 25 (2013), Article ID 110803. Available at http://dx.doi.org/10.1063/1.4818981.

[32] S.B. Pope and R. Gadh, *Fitting noisy data using cross-validated cubic smoothing splines*, Commun. Stat. Simul. Comput. 17 (1988), pp. 349–376.

[33] M. Muradoglu, S.B. Pope and D.A. Caughey, *The hybrid method for the PDF equations of turbulent reactive flows: consistency conditions and correction algorithms*, J. Comput. Phys. 172 (2001), pp. 841–878.

Appendix A.   Mesh-free particle method

A mesh-free particle method is used to obtain numerically-accurate solutions to the LES/PDF equations for the random-walk model in the DNS limit applied to the idealised, unstrained, 1D, plane laminar flame. The equations are solved in the frame in which the reactants are at rest at $x = -\infty$. From a specified initial condition, the solution is advanced in time through small time steps Δt, and eventually reaches a fully-developed state, with the flame moving to the left at a constant speed u_F. The solution domain extends from pure reactants to pure products, and is moved with the flame.

There are a large number N of particles, the nth having position $X^{(n)}(t)$ and composition $\phi^{(n)}(t)$ at time t. The solution is advanced from time t to time $t + \Delta t$ through the following sequence of operations (with some details to follow). Prior to the start of each step, the particles are sorted in position so that $X^{(n)} \geq X^{(n-1)}$.

(1) The particle diffusivities are evaluated, and the mean diffusivity at the particle locations, $\widetilde{\mathcal{D}}^{(n)}$, is estimated using a cross-validated smoothing linear spline.
(2) The mixing rate $\widetilde{\Omega}^{(n)}$ is determined from $\widetilde{\mathcal{D}}^{(n)}$.
(3) The mixing sub-step is performed using the near-neighbour implementation of the IEM model [31].
(4) The reaction sub-step is performed.
(5) The particles are moved by the diffusion term of the random walk, and then re-sorted.
(6) The particles are moved by the drift term in the random walk.
(7) As necessary, the domain is moved, and particles are removed and added as necessary at the boundaries.

In order to estimate means, the particles are partitioned into odd and even-numbered particles. Linear smoothing splines [32] (with smoothing parameter s) are generated based on the two sets of particles, and the cross-validation error $\chi(s)$ is computed. An iteration is performed to determine the value of the smoothing parameter that minimises the error. (For computational efficiency, if there are a large number of particles, then this procedure is applied, not to individual particles, but to clusters of adjacent particles. Here the number of clusters is limited to 1000.)

The particles move due to the drift term in the random walk (Equation 8) according to $dX^*/dt = [\widetilde{U} + \widetilde{v}\nabla(\langle\rho\rangle\widetilde{\mathcal{D}})]^*$. Fortunately, however, this drift coefficient does not need to be evaluated, because the effect of the drift can be implemented implicitly by enforcing a consistency condition [33]. Every

particle is ascribed the same mass per unit cross-sectional area, m''. The nth particle, with specific volume $v^{(n)}$, therefore has a length associated with it of $\ell^{(n)} = m''v^{(n)}$. The consistency condition is that the particle length is equal to the geometric length that the particle occupies. This condition is strongly enforced by (at the end of the time step) setting the particle positions by

$$X^{(n+1)} = X^{(n)} + \frac{1}{2}[\ell^{(n+1)} + \ell^{(n)}]. \tag{A1}$$

The solutions reported in Section 4.5 are performed with $N = 10^5$ particles, which is more than needed to produce very accurate results. Tests are performed to ensure that the time step Δt is sufficiently small, and the simulation duration sufficiently long, so that the associated numerical errors are negligible.

Appendix B.   Cloud-in-cell particle/mesh method

The cloud-in-cell (CIC) particle/mesh method is applicable to both the random-walk and the mean-drift models, and is similar to the method generally used in LES/PDF simulations.

As in the mesh-free method, there are N computational particles. There is also a mesh of uniform spacing h. There is a linear-spline basis function associated with each mesh node. Means are estimated at the nodes using kernel estimation with the basis functions as the kernels, and then the means are represented by linear splines.

The differences compared to the mesh-free method are as follows.

(1) All means are estimated and represented using the CIC linear basis functions.
(2) The IEM mixing model is implemented directly using the CIC means $\widetilde{\Omega}$ and $\widetilde{\phi}$ by integrating the equation

$$\frac{\mathrm{d}\phi^*}{\mathrm{d}t} = -\Omega^*(\phi^* - \widetilde{\phi}^*). \tag{B1}$$

(3) The mean drift is implemented by

$$\phi^*(t + \Delta t) = \phi^*(t) + [\widehat{\phi}(t + \Delta t) - \widehat{\phi}(t)]^*, \tag{B2}$$

where $\widehat{\phi}(x, t + \Delta t)$ is the solution after time Δt of the partial differential equation

$$\frac{\partial \langle\rho\rangle\widehat{\phi}}{\partial t} = \frac{\partial}{\partial x}\left(\langle\rho\rangle\widetilde{\mathcal{D}}\frac{\partial\widehat{\phi}}{\partial x}\right), \tag{B3}$$

from the initial condition $\widehat{\phi}(x, t) = \widetilde{\phi}(x, t)$. Equation (B3) is integrated numerically at the nodes, using a fully implicit three-point difference scheme.